

Investigating the Effects of ACF Spray Angle and Distance on its Performance for Micro-Drilling

ME451 Project Final Report

Ayano Hiranaka

December 10, 2019

Abstract

Cutting fluids are liquids, commonly water or oil-based, used as coolants and lubricants during machining processes. While these liquids are often harmful to the environment, traditional methods to apply cutting fluids to the machining tool require large amounts of fluids for each machining operation. In contrast to the traditional methods, atomization-based cutting fluid (ACF) spraying system applies a spray containing micro-sized droplets of the fluid to the cutting interface. Because these droplets are small enough to penetrate the interface and cool the tools locally, the amount of fluid used for a machining operation is significantly smaller. Past efforts have been made to optimize the use of ACF systems in micro-turning and micro-end milling, but the study concerning micro-drilling is lacking. The goal of this project is to investigate the effects of spray distance and angle on the performance of the ACF system for a micro-drilling operation.

Four combinations of spray angles and spray distances are tested to investigate the effects of these ACF spray parameters on cutting force, torque, and tool life on micro-drilling. Results suggest that the effects of spray distance and angle are small on cutting force, drilling at shorter spray distance result in higher torque, and shorter spray distance and a less-horizontal spray angle result in the longest tool life.

However, because the collected data is highly variable, additional experimentation are needed to confirm these observations.

1. Introduction

In micro-manufacturing, high tool speed often causes chips to stick to the tool-material interface, causing tool failure or poor machining quality, and an optimized use of ACF systems can contribute to solving this problem [8]. Effective cutting fluid application in micro-machining is characterized by low cutting force, long tool life, good chip evacuation, high machining quality, and low cutting temperature. An important spray parameter to ensure chip evacuation is droplet velocity. While higher velocity result in

more effective chip removal, velocities that are high enough may cause splashing, preventing effective wetting [2]. Effective spreading of the fluid on the cutting interface leads to improved cutting force and temperature. Previous research by Ganguli concluded that, for effective spreading, conditions

$$We > 10 \text{ and } K_m = \left(Oh^{-\frac{2}{3}} We \right)^{5/8} < 57.7$$

must be met, where We is the Weber number and Oh is the Ohnesorge number [4]. Splashing results when these conditions are not met, reducing fluid effectivity. The range of allowed droplet velocities to meet these conditions is dependent on the droplet diameter. Tanveer, in his study, concluded that droplet diameters between 12.5 and 30 μ m ensure spreading without splashing for a wide range of droplet velocities [7], making these values a good target value for droplet diameters. To control the droplet diameter, it is important to understand the factors that influence the parameter. In an ACF system, the droplet diameter is dependent on the atomizer parameters. In a study investigating the effects of droplet diameter on heat exchange for a MQCL system, Maruda states that higher airflow and longer nozzle distance results in smaller droplet diameter. This relation is described by

$$D_{avg} = 14.8l^{-0.681}p^{-0.438},$$

where l is the distance in meters between atomizer nozzle and cutting zone, and p is the volumetric air flow within the atomizer in L/min [1]. Rajan proposes an alternate relation to estimate the droplet diameter that takes additional factors, such as atomizer frequency, power, vibrating area, and liquid properties, into consideration [5].

Previous research on the effects of ACF spray parameters on its performance have been conducted for micro-turning and micro-end milling applications. In a study investigating the effects of spray parameters on the turning of Titanium alloy, Nath reports that the combination of low gas pressure, long spray distance, and high droplet flow rate resulted in the longest tool life [3]. Additionally, in a study investigating the effects of MQL parameters on cutting force and temperature during end-milling of Titanium alloys, Liu discovered that a spray distance of 25 mm resulted in the lowest cutting force and temperature, while the spray angle had minimal effect on penetration ability, cutting force, and temperature [6]. Study on the effects of spray parameters on micro-drilling operations are however lacking and is the focus of this study.

2. Experimental Design: Theoretical

The following sections discuss the physical setup and the variables of the experiment determined theoretically from calculations, assuming ideal spray behaviors (linear trajectory with uniform droplet diameters).

2.1 Experimental Setup

The initially proposed experimental setup is shown in Figure 1. Dimensions X_o , Z_o , and L are constants, and their values are measured to be 115, 230, and 123 mm, respectively. Spray angle θ and spray distance Δx are independent variables in the experiment. The geometric constraint of the setup limits Δz to between 82 and 165 mm. A digital angle gauge is attached to the atomizer to set the spray angle accurately. The CNC machine supplies cutting fluid to the atomizer, and an external air valve is used to supply air flow to the atomizer.

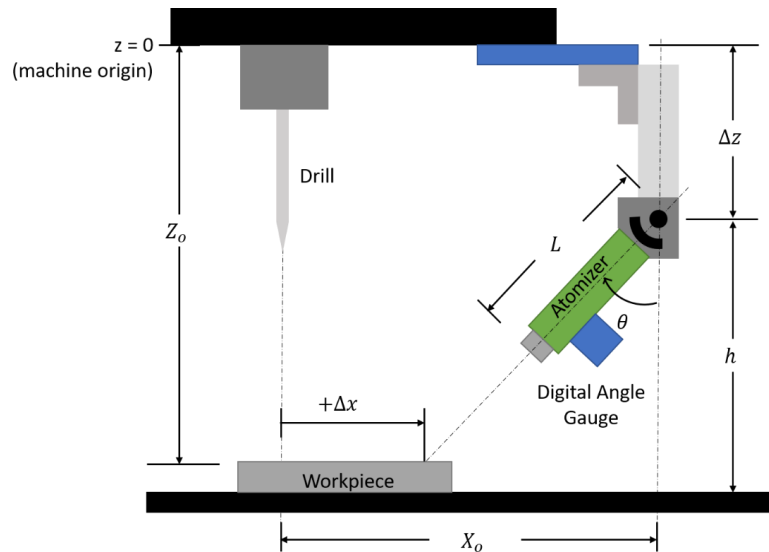
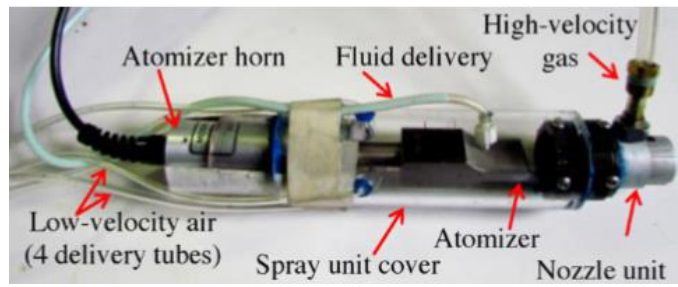
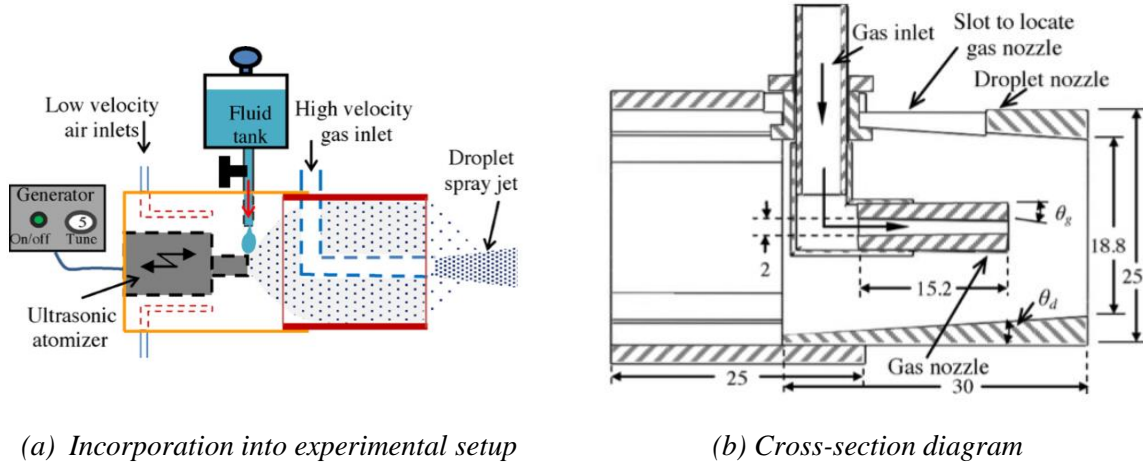


Figure 1: Experimental Apparatus

The atomizer used in the experiment is VC5040AT from Sonic and Materials, Inc., identical to that used in Nath's study. Atomizer vibrates at 40 kHz and produce droplets around 50 μm at maximum flow rate of 10 L/hour [3]. Details of the atomizer is described in Figure 2.



(c) Photograph of atomizer

Figure 2: Ultrasonic Atomizer [3]

The cutting fluid and the material used are S-1001 10% and Starvax stainless steel, respectively. Its properties are summarized in Tables 1 and 2.

Table 1: Properties of S-1001 10% [3]

Surface Tension [mN/m]	Density [kg/m ³]	Viscosity [cP]	Thermal Conductivity [W/m K]
41	1003	1.22	0.53

Table 2: Properties of STAVAX [12]

Density [kg/m ³]	Modulus of Elasticity [MPa]	Thermal Conductivity [W/m °C]	Specific Heat [J/kg °C]	Tensile Strength [MPa]	Yield Strength [MPa]
7800	200,000	19	460	1780	1460

2.2 Combinations of Spray Angles and Distances

In order to study the effects of spray distance and angle, two different values for each parameter will be tested for a total of four experimental conditions. Two distances, close to the tool and away from the tool,

to be tested are 5 and 15 mm, respectively. The range of possible spray distance values are determined for spray angles between 10 and 70 degrees using the following relation defined from Figure 1:

$$\Delta x = X_o - (Z_o - \Delta z)\tan\theta.$$

Note that a positive spray distance corresponds to the situation in which the spray reaches the target on the atomizer side of the drill axis, and a negative spray distance corresponds to the spray surpassing the drill axis (as defined in Figure 1). The calculation results shown in Figure 3 reveal that spray angle values between 55 and 65 degrees allow spray distances of both 5 and 15 mm. Two spray angles to test are determined to be 55 and 65 degrees. The four testing conditions and corresponding atomizer height Δz values are summarized in Table 3.

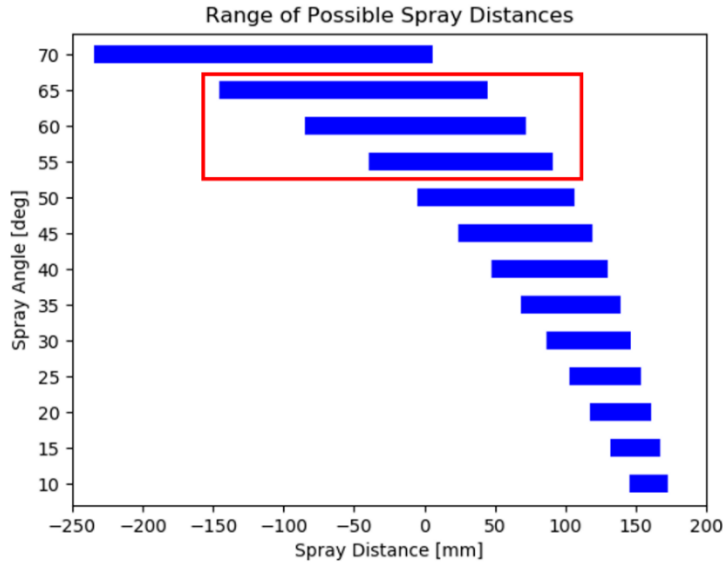


Figure 3: Range of Possible Spray Distances for Various Spray Angles

Table 3: Summary of Test Conditions and Corresponding Atomizer Height

Spray Angle [deg]	Spray Distance [mm]	Corresponding Δz [mm]
55	5	109
55	15	116
65	5	149
65	15	154

3. Experimental Design: Actual

Two major problems arose when experimenting with the devices, making some parts of the experimental setup proposed in section 2 impractical:

- 1) The spray is not linear nor uniform as previously assumed. As illustrated in Figure 4, droplets further away from the atomizer device are finer and the trajectory is parabolic, preventing the spray to reach the drilling interface when the atomizer angle and distance are set to combinations from Table 3. The small distance between the atomizer and the drill places a tight constraint on the possible angle-distance combinations. Two distinct combinations in which the spray reach the drilling interface cannot be obtained with the setup (for any given height, the possible range of spray angles was around 5 degrees).
- 2) Cutting fluid flow rate is too high, resulting in the atomizer output to be a stream rather than a spray, regardless of the air flow and atomizer amplitude settings.

The following sections describe the changes made to the experimental setup to overcome these problems.

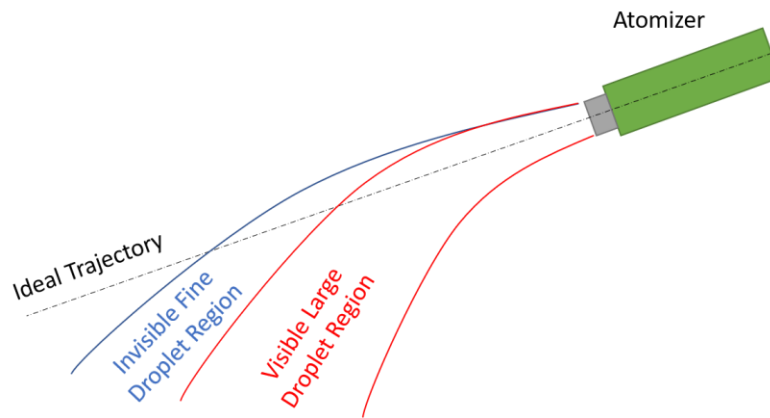


Figure 4: Ideal and Observed Spray Behaviors

3.1 Modifications to Physical Setup

To solve the first problem, the atomizer assembly is detached from the drill base and is placed onto an external mount to increase the distance between the atomizer and drill. This expands the allowable range of spray angles. Additionally, the mounting structure has height adjustment, and a built-in scale allows direct measurement of atomizer height. The high cutting fluid flow rate problem is solved by supplying the fluid through a tank. The flow rate can be adjusted by using a valve placed onto the tube connecting the tank to the atomizer. The revised experimental setup is shown in Figure 5.

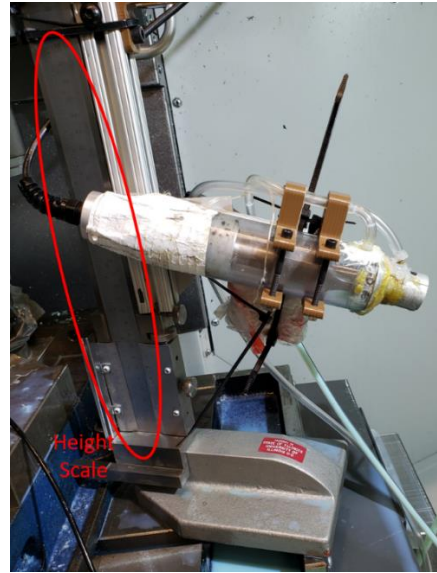
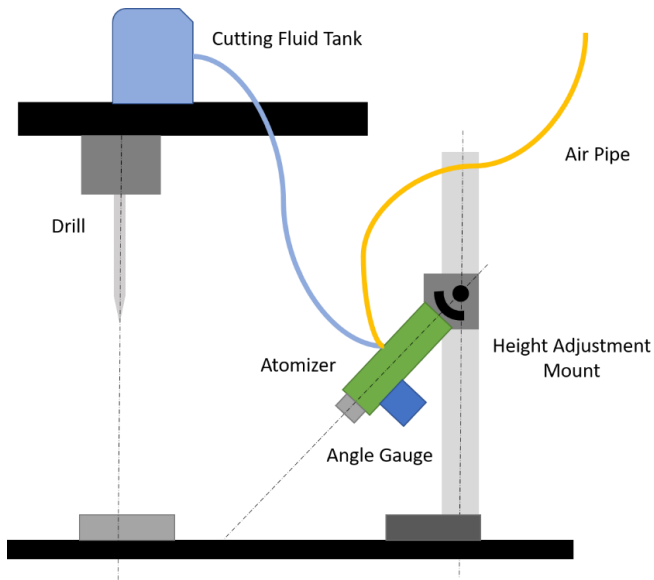


Figure 5: Revised Experimental Setup

3.2 Modifications to Spray Angle-Distance Combinations

Given the change in spray behavior and physical setup, the spray angle and distance combinations are also revised. Two new spray angles (73 and 83 degrees) are selected, and for each spray angle, two drill locations, close to the spray and away from the spray, are tested as shown in Figure 6 and Figure 7. Table 4 summarizes the test conditions. The larger and smaller spray distances for each spray angle correspond to “Drill Location A” and “Drill Location B,” respectively in Figures 6 and 7. The drill’s orientation with respect to the spray for each spray angle and spray distances are shown in Figure 8.

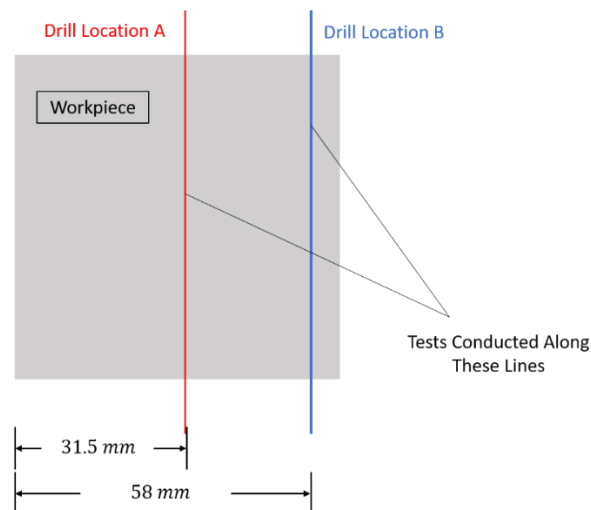


Figure 6: Drill Locations

Table 4: Revised Spray Angle and Distance Combinations

Spray Angle [deg]	Corresponding h [mm]	Horizontal Distance [mm]*	Spray Distance [mm]**
73	104	90	120
73	104	32	71
83	76	85	103
83	76	27	65

*horizontal distance between the end of the atomizer to the point of contact between the workpiece and the drill

**straight-line distance between the end of the atomizer and the point of contact

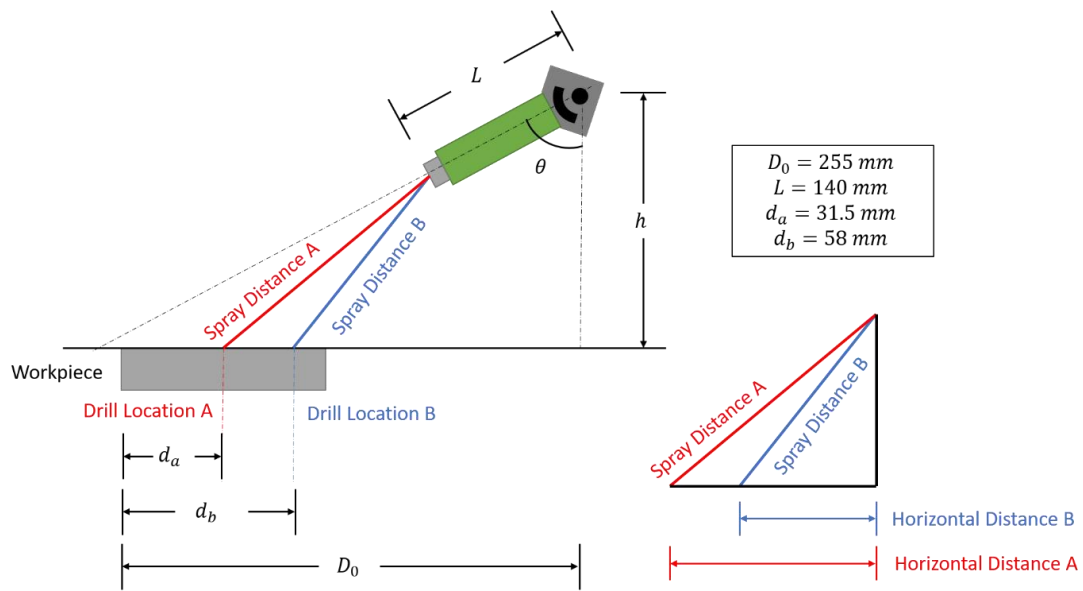


Figure 7: Final Experimental Setup and Test Conditions



(a) Location A, 73 degrees



(b) Location B, 73 degrees



(c) Location A, 83 degrees



(d) Location B, 83 degrees

Figure 8: Spray Profiles Corresponding to Each Test Condition

3.3 Experimental Procedures

The control variable used in the experiment are summarized in Table 5 and the experimental procedures are outlined below:

- 1) Load a drill bit onto the machine, taking care not to damage the tool.
- 2) Set the atomizer to the first angle and height using the digital angle gauge reading.
- 3) Set the air pressure and atomizer amplitude.
- 4) Set drill position corresponding to the first test condition.
- 5) Fill the cutting fluid tank to a set height (because the cutting fluid is being provided by a tank, the spray profile exhibits significant variation depending on the amount of fluid remaining in the tank).
- 6) Confirm that the spray is steady and is reaching the drilling interface. Record the spray profile.
- 7) Drill to the desired depth while collecting force and torque data.
- 8) Replace the drill bit, then repeat steps 4 to 7 until all test conditions using the current spray angle are complete.
- 9) Set the atomizer to the next angle and height, then repeat steps 4 to 8.

Table 5: Summary of Control Variables

Air Pressure [psi]	Atomizer Amplitude	Tool Speed [RPM]	Feed Rate [mm/min]	Drill Depth [mm]
14.5	525	2000	16	7.5

4. Drill Parameter Measurements

The following measurements are made on each of the 50 drill bits: (1) diameter, (2) web thickness, (3) land, (4) point angle, (5) helix angle, and (6) flute length. All images are taken using the Optical Digital Comparator. Additionally, for all measurements excluding flute length, image processing is performed

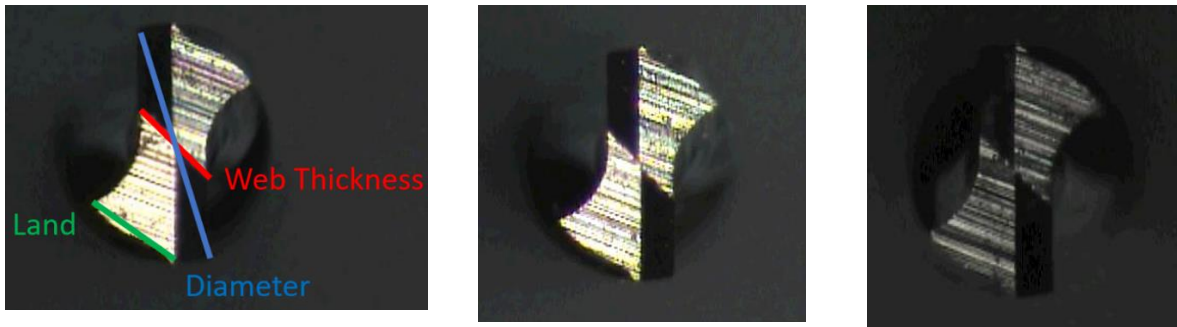
using Python OpenCV to obtain the measurements in pixels. All images are taken at x4.5 magnification, and the pixel measurements obtained through image processing is converted to micron measurements using the following conversion factor:

$$measurement [\mu m] \approx 2.174 * measurement [pixels].$$

The 2.174 factor is determined from an image of a calibration slide taken at x4.5 magnification (230 pixels corresponded to 0.5 mm). The following sections describe the methods used to obtain each measurement.

4.1 Diameter, Web Thickness, and Land

A sample image used to obtain diameter, web thickness, and land, with these dimensions marked, is shown in Figure 9a. While some images, such as one in Figure 9b, exhibit high contrast and show clear edges and vertices, other images, such as one in Figure 9c, have low brightness, making edges and vertices difficult to identify.



(a) Sample image and measurements to be taken from the image (b) Example of good image (c) Example of bad image

Figure 9: First Image Taken for Each Bit and Measurements to be Taken from the Image

An ideal way to measure the diameter is to identify the endpoints of the blue line in Figure 9a and calculate the distance between them. However, these two points are not identifiable in many of the dark images. In contrast, the geometry that appear bright in the image is simpler to identify, and therefore the bright portions of the image are used for the diameter, web thickness, and land calculations. To extract the bright geometry, all images are processed in the following way prior to making any measurements.

- 1) Image brightness is adjusted as needed to make the brightness more uniform among all images (for example, brightness for the image in Figure 9c is increased).
- 2) A Gaussian blur is applied to each image to make the stripes seen on the image less prominent.
- 3) Each image is cropped, and a brightness threshold is applied to convert the image into a binary image.
- 4) A series of erosions and dilations are applied to each binary image to eliminate noise.

5) OpenCV function *findNonZero* is used to find coordinates of all white pixels in the binary image.

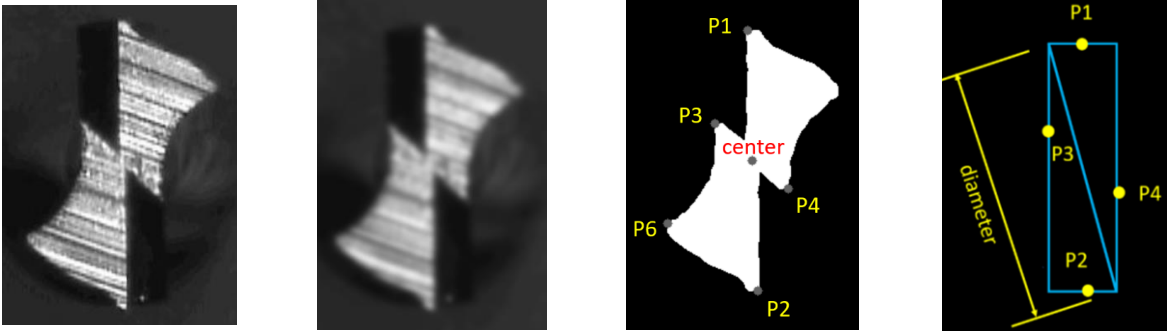
After the pre-processing, the diameter, web thickness, and land are calculated in the following manner:

- 1) Refer to Figure 10c. P1 is identified as the upper-most point among the points identified in (5). Similarly, P2 is identified as the lower-most point.
- 2) The center of the bit is approximated to be the midpoint between P1 and P2.
- 3) Algorithm 1 is used to identify P3. P4 is identified using Algorithm 1 with slight modifications.
- 4) The diameter is calculated using the coordinates of P1, P2, P3, and P4. Namely:

$$diameter = \sqrt{|x_3 - x_4|^2 + |y_1 - y_2|^2},$$

where x_n and y_n are the x and y coordinates of point n , respectively (x is horizontal axis, y is vertical axis).

- 5) The web thickness is calculated as the distance between P3 and P4.
- 6) P6 is identified as the left-most white point (P6 may also be the right-most point. The left-most point was selected because the left point was more clearly visible in the images taken).
- 7) Land is calculated as the distance between P2 and P6.



(a) Cropped Image

(b) Blurred Image

(c) Points Identified

(d) Drill Diameter

Figure 10: Diameter, Web Thickness, and Land Calculation Process

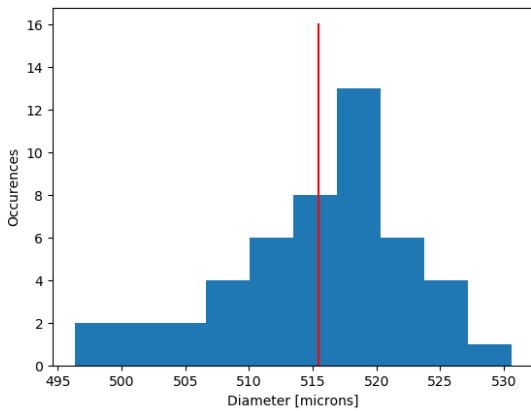
Algorithm 1: Identification of P3

Let (x_c, y_c) be coordinates of the drill center, and *whitepix* be a list containing the coordinates of all white pixels within the binary image.

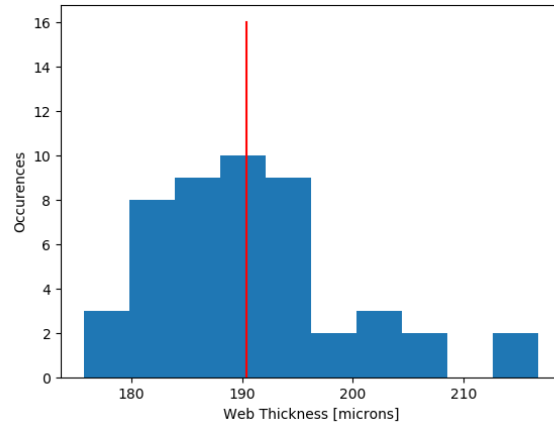
1. Within *whitepix*, find all points in the same row as the center. That is, their y -coordinate is y_c . Identify the left-most point within this group. If the horizontal displacement between this point and the center is greater than a threshold (e.g. 10 pixels), this value is potentially P3.

2. Repeat 1 for one row above the center. If a new potential P3 is identified, update it.
 3. Continue to iterate, moving one row up each time, until there is no longer a white pixel to the left of the drill center. The last identified potential P3 is determined to be P3.
-

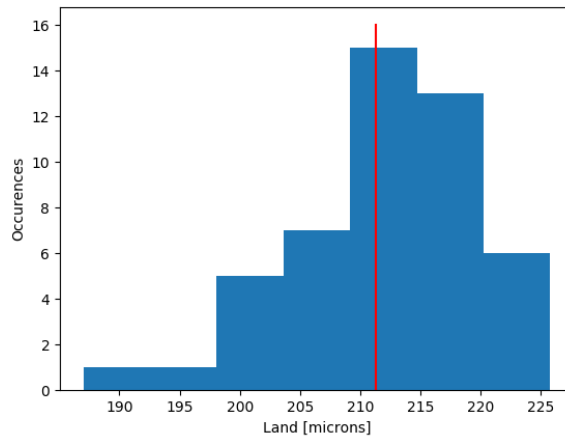
The Python functions used to for the above calculations is provided in the appendix. The distribution of the calculated diameter, web thickness, and land are shown in Figure 11, with the mean values indicated with a red line. The mean values of the diameter, web thickness, and land are 515.47, 190.38, and 211.26 μm , respectively. The standard deviations are 7.26, 8.81, and 7.52 μm , respectively.



(a) Diameter



(b) Web Thickness



(c) Land

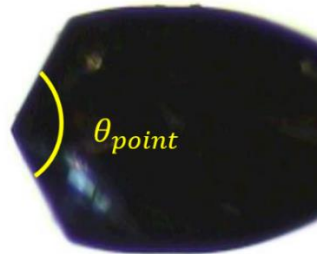
Figure 11: Distribution of Calculated Diameter, Web Thickness, and Land

4.2 Point Angle

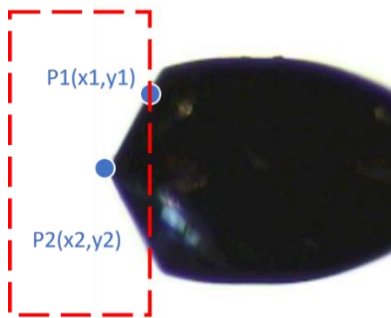
Figure 12a shows a sample image used to calculate the point angle, with the point angle labeled. Assuming that the drill is symmetric about its rotational axis, the point angle can be calculated if the

coordinates of two points on the angled edge are determined, as shown in Figure 12b, with the following equation:

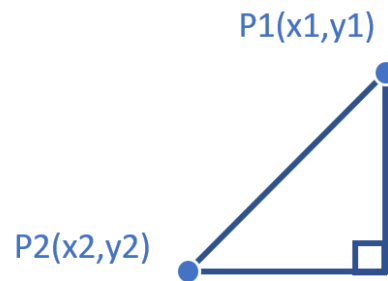
$$\theta_{\text{point}} = 2 \tan^{-1} \left(\left| \frac{y_2 - y_1}{x_2 - x_1} \right| \right).$$



(a) Sample image and point angle



(b) Two points used to calculate point angle



(c) Geometry used to calculate point angle

Figure12: Point Angle Calculation

To obtain the necessary point coordinates the following method is used:

- 1) Image is cropped at the red dashed line in Figure 12b to include the tip only.
- 2) Cropped image is inverted (bit becomes white, background becomes black), and a brightness threshold is applied to convert the image to binary.
- 3) OpenCV function *findNonZero* is used to find the coordinates of all non-black pixels in the image.
- 4) Find the pixel with the smallest x coordinate value (P1) and the pixel with the largest y coordinate (P2).

The function used to calculate the point angle from an input image is included in the appendix, and the distribution of the calculated point angle values is shown in Figure 13 (mean value is marked with a red line). The mean and standard deviation are 125.22 and 2.67 degrees, respectively.

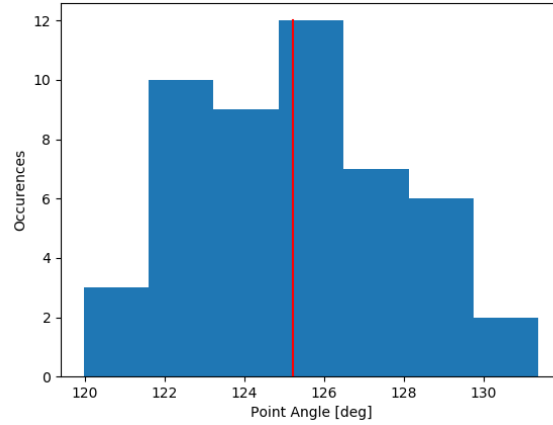


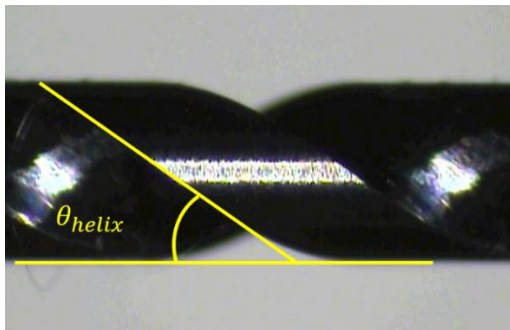
Figure 13: Distribution of Calculated Point Angle Values

4.3 Helix Angle

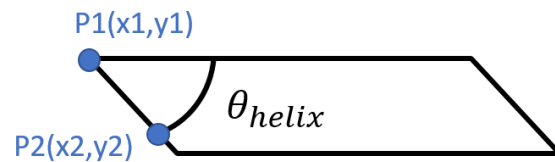
A sample image used to calculate the helix angle is shown in Figure 14a. The parallelogram-shaped shine is used to calculate the helix angle using a method like the one used to calculate the point angle. As shown in Figure 14b, the acute angle of the shine can be approximated as the helix angle, and the coordinates of two points on the slanted edge can be used to calculate the angle as:

$$\theta_{\text{helix}} = \tan^{-1} \left(\left| \frac{y_2 - y_1}{x_2 - x_1} \right| \right).$$

However, as shown in the masked image in Figure 14c, the vertex could not be clearly extracted, requiring additional steps to obtain two points on the slanted edge, as shown in Figure 14d.



(a) Sample microscope image



(b) Shape of shine and helix angle equivalent



(c) Masked image of shine corner



(d) Identified $P1$ and $P2$ on masked image

Figure 14: Image Processing for Helix Angle Calculation

Below is a summary of the method used to calculate the helix angle. The complete function used for the calculation can be found in the appendix.

- 1) Image is cropped to extract the corner of the parallelogram-shaped shine.
- 2) A brightness threshold is applied to convert the image to binary (only the shine remains white).
- 3) Coordinates of all white pixels are found using the *findNonZero* function.
- 4) $P1$ is obtained by finding 50 points with the smallest x values, then finding the point with the largest y value within the 50 points.
- 5) $P2$ is obtained by finding 50 points with the largest y values, then finding the point with the smallest x value within the 50 points.

The measurements obtained are shown in Figure 15, with the mean value marked with a red line. The mean and standard deviation of the measurements are 36.27 and 1.26 degrees, respectively.

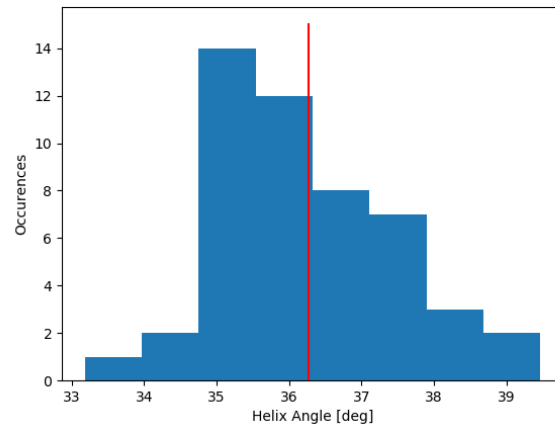


Figure 15: Distribution of Calculated Helix Angle Values

4.4 Flute Length

The flute length, or the distance from the tip of the drill to the end of the flutes, is measured directly using the microscope's measuring function. The measurement distribution is shown in Figure 16. The mean and the standard deviation of the measurements are 7.816 and 0.0083 mm, respectively. The minimum flute length (limiting factor for depth of drilling) is 7.796 mm.

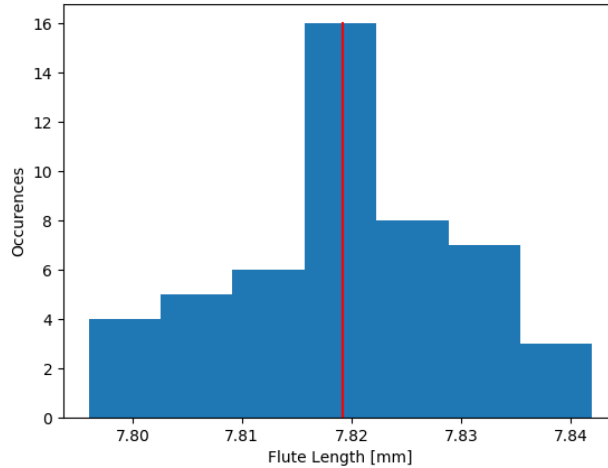


Figure 16: Distribution of Measured Flute Length Values

4.5 Comparison of Measurements to Nominal Values

Table 4 summarizes the measured and nominal drill parameters. Error is calculated as:

$$Error = \frac{|measured - nominal|}{nominal} * 100\%.$$

Table 6: Comparison of Measured and Nominal Drill Parameters

	Measured (Average)	Nominal*	% Error [%]
Diameter [μm]	515.47	500.38	3.016
Web Thickness [μm]	190.38	-	-
Land [μm]	211.26	-	-
Point Angle [deg]	125.22	135	7.244
Helix Angle [deg]	36.27	35.00	3.629
Flute Length [mm]	7.816	7.874	0.737

*Nominal dimensions from Performance Micro Tool catalog [12]. Official information is not available for nominal web thickness and land dimensions.

High error is observed in the point angle measurements. To understand this discrepancy, five additional point angle images are taken for randomly selected drill bits. For each image, the point angle is measured

both with the Digital Optical Comparator and the method explained in section 4.2. Results are summarized in Table 7. The error in the retaken images is 0.01%; Significantly lower than error in the original data set. This suggests that high error in the initial dataset resulted from the orientation at which the bits were placed when the images were taken (rotating the bit changes the observed angle).

Table 7: Additional Point Angle Measurements

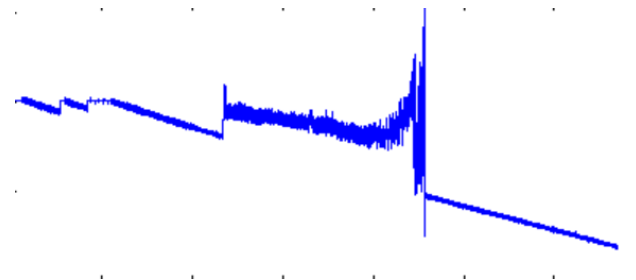
Image #	Measurement from Comparator [deg]	Measurement from Image Processing [deg]
1	136.1	137.7
2	133.7	135.8
3	132.8	134.5
4	134.5	136.4
5	135.2	137.4
Average	134.46	136.36
% Error [%]	0.004	0.01

5. Results and Discussions

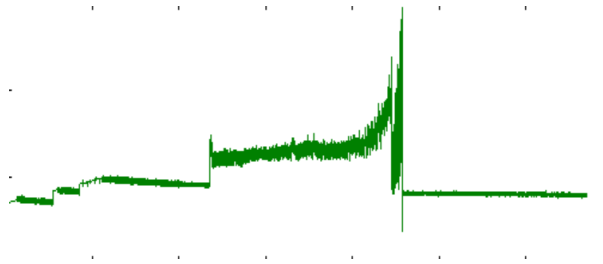
For each drilling operation, cutting force and torque data are collected using LabView at a rate of 4000 data points per second. The collected data are then processed and evaluated.

5.1 Data Preprocessing

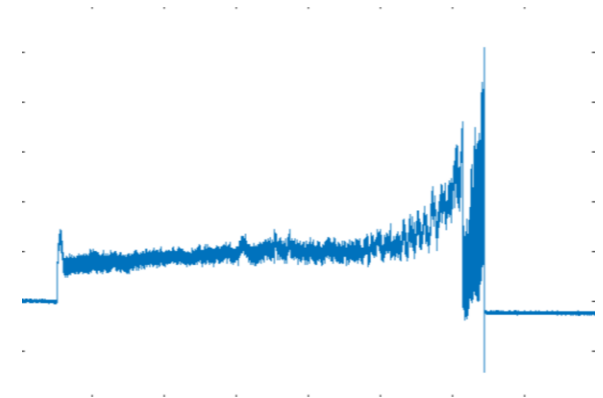
Before evaluating the cutting force and torque, data for each test condition are preprocessed. First, for both the force and torque data, a second order polynomial approximating the drift is determined. The drift is then corrected by subtracting the polynomial from the data. In addition, since the torque data exhibited high noise, Savitzki-Golay filter is applied to elucidate the trend. Finally, the point at which the drilling began is identified from the force plots. Both the force and torque data are cropped from when the bit is 0.5 mm above the workpiece to until the end of the drilling operation (corresponding to a depth of 8.0 mm). An example of preprocessing is shown in Figure 17, and an example MATLAB code used in the preprocessing is found in the Appendix.



(a) force plot prior to processing



(b) force plot with drift removed



(c) force plot after all preprocessing

Figure 17: Example of Data Preprocessing

5.2 Effects on Cutting Force

To investigate the effects of spray distance on cutting force, the average cutting force for each experiment is approximated by taking the mean cutting force for a section where drilling is in steady state, as shown in Figure 18. The estimated average cutting force for each experiment is summarized in Table 8. The average cutting force for all short spray distance cases, long spray distance cases, 73-degree cases, and 83-degree cases are 11.03, 11.13, 11.50, and 10.73 N, respectively. Within the range of spray angles and spray distances tested in this experiment, average force values are similar for all test cases, and no significant relationship between average force and spray distance or spray angle is observed. Figure 19 compares the force history for test cases by each spray angle. Figure 19 shows the force history for all experiments.

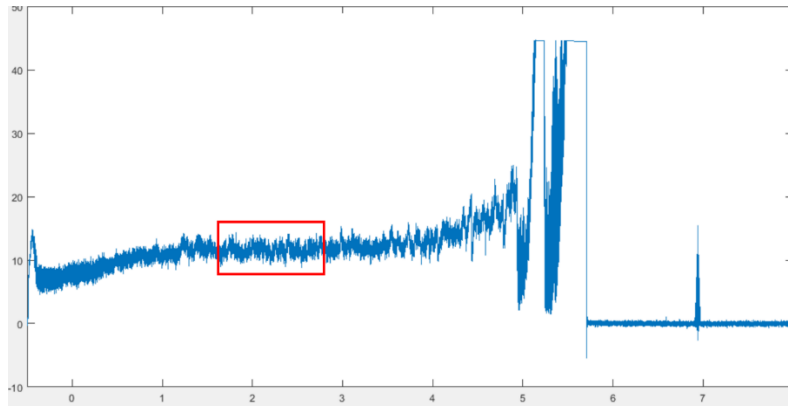
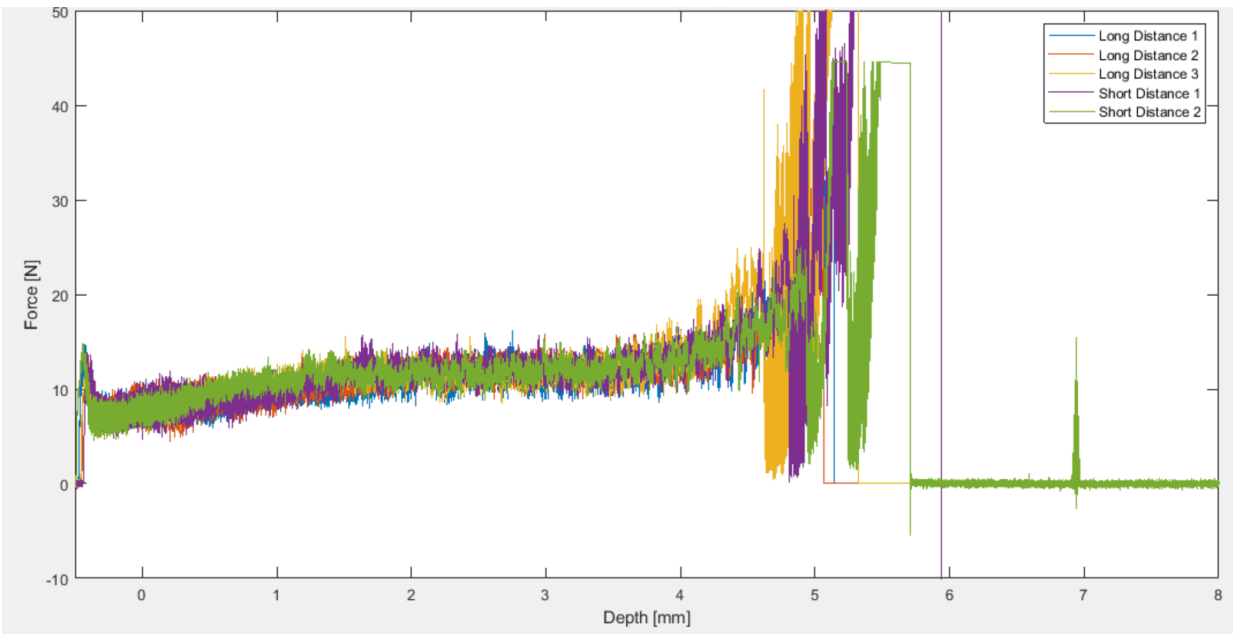


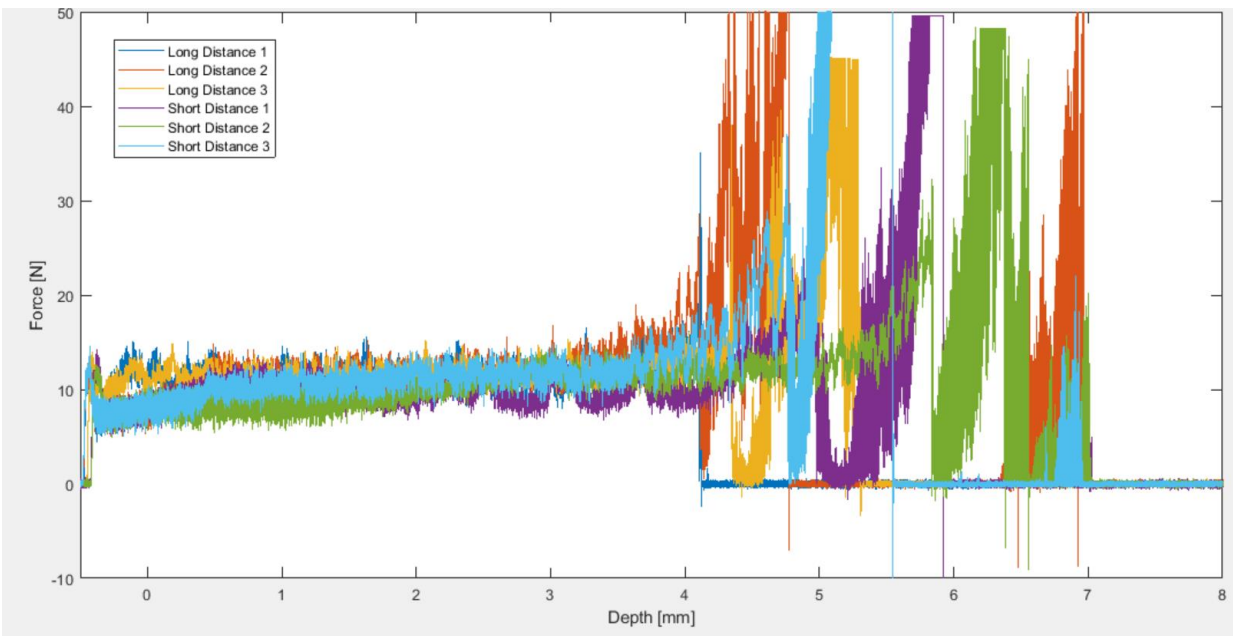
Figure 18: Average Cutting Force

Table 8: Average Cutting Force for All Experiments

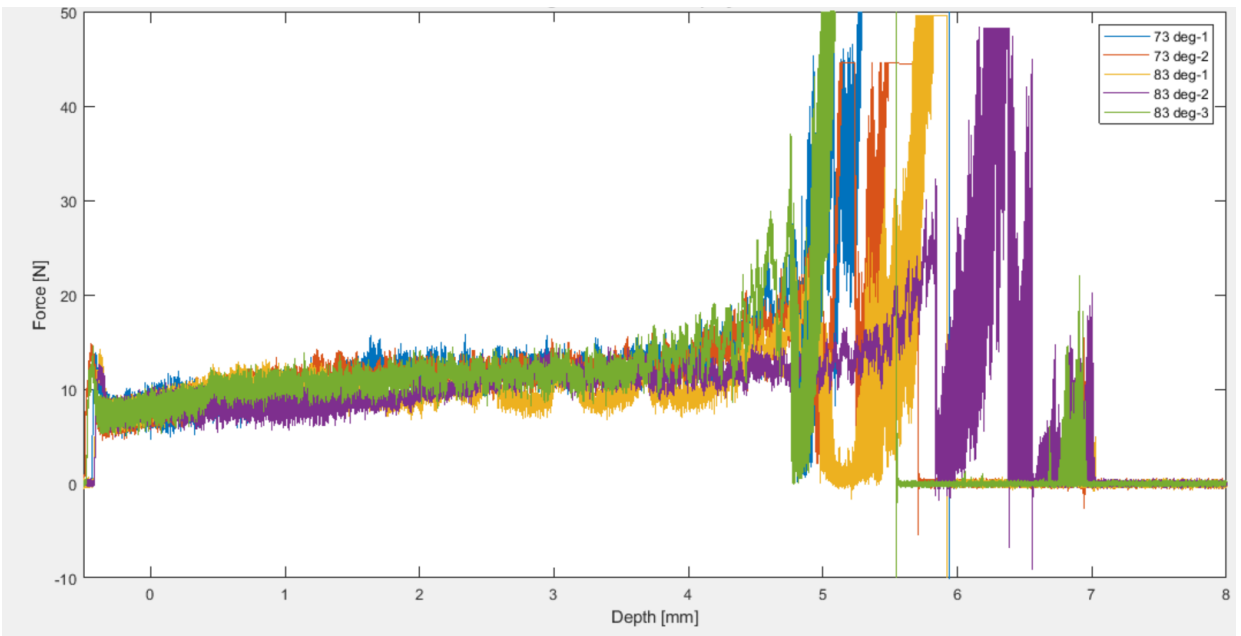
Experiment #	Spray Angle [deg]	Spray Distance	Average Force [N]
1	73	Short	11.89
2	73	Short	11.13
3	73	Long	11.53
4	73	Long	11.62
5	73	Long	11.43
6	83	Short	9.68
7	83	Short	11.43
8	83	Short	11.02
9	83	Long	9.46
10	83	Long	11.21
11	83	Long	11.62
Short Distance Average			11.03
Long Distance Average			11.13
73 degrees Average			11.50
83 degrees Average			10.74



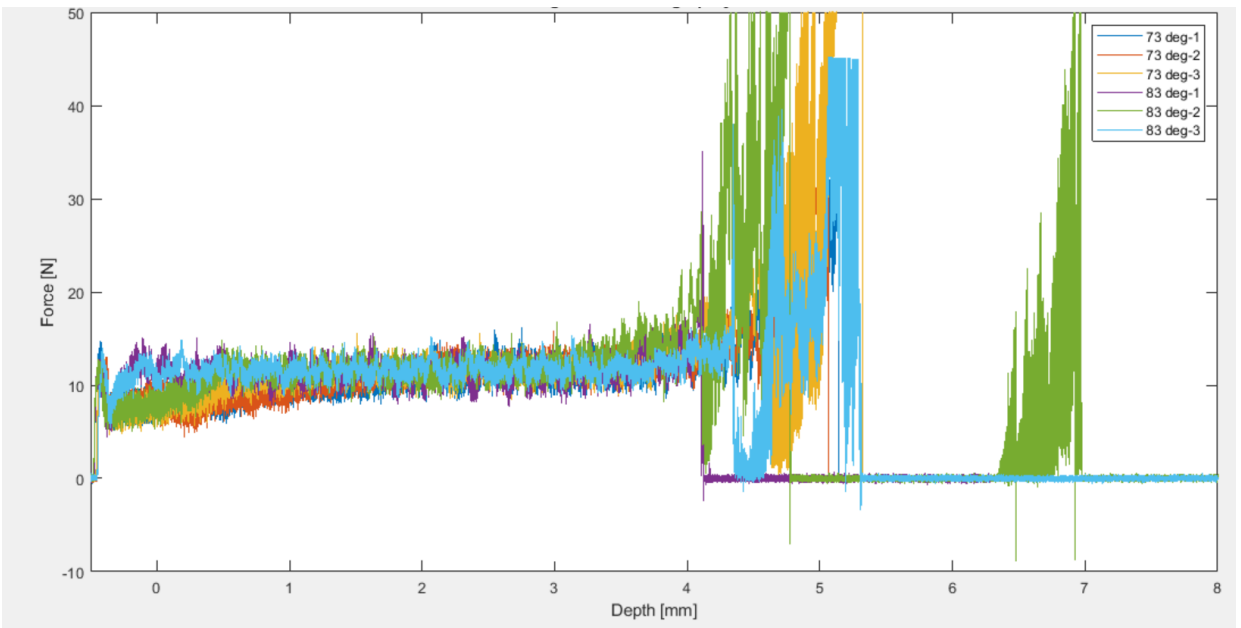
(a) Spray Angle 73 degrees



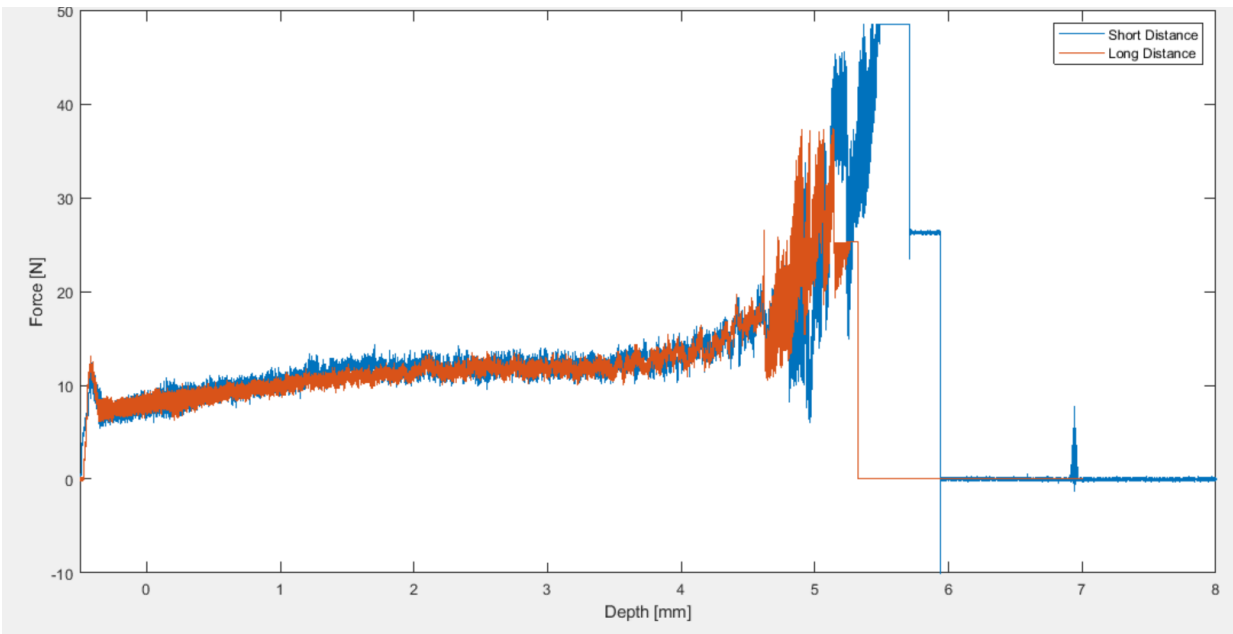
(b) Spray Angle 83 degrees



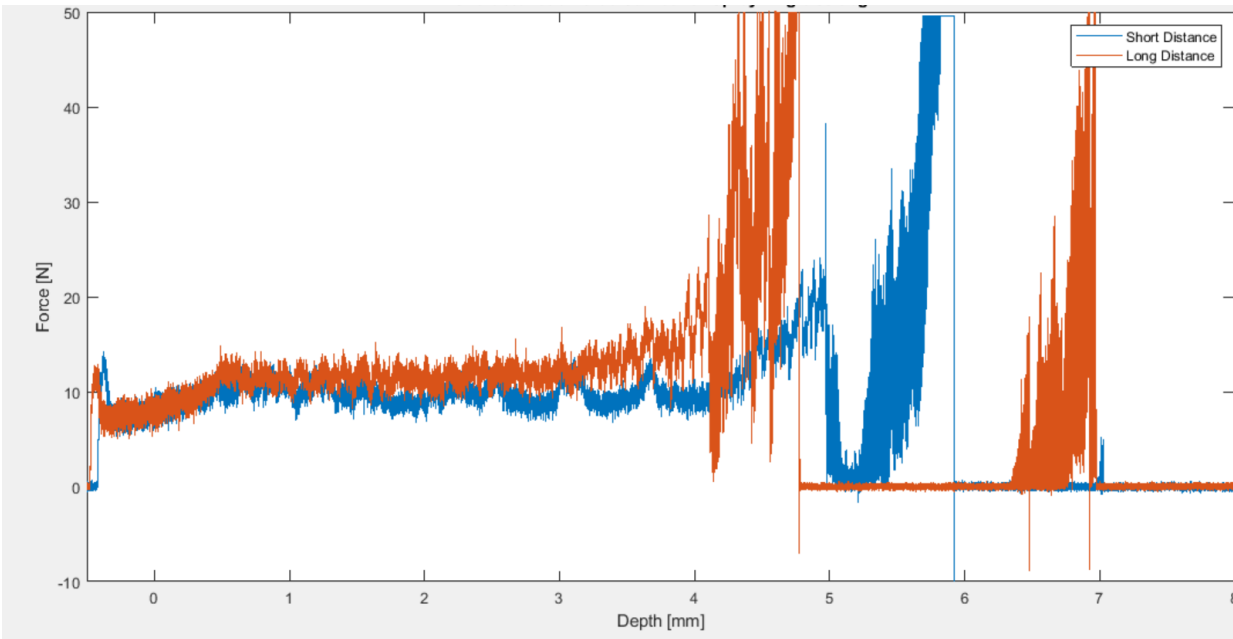
(c) Short Spray Distance



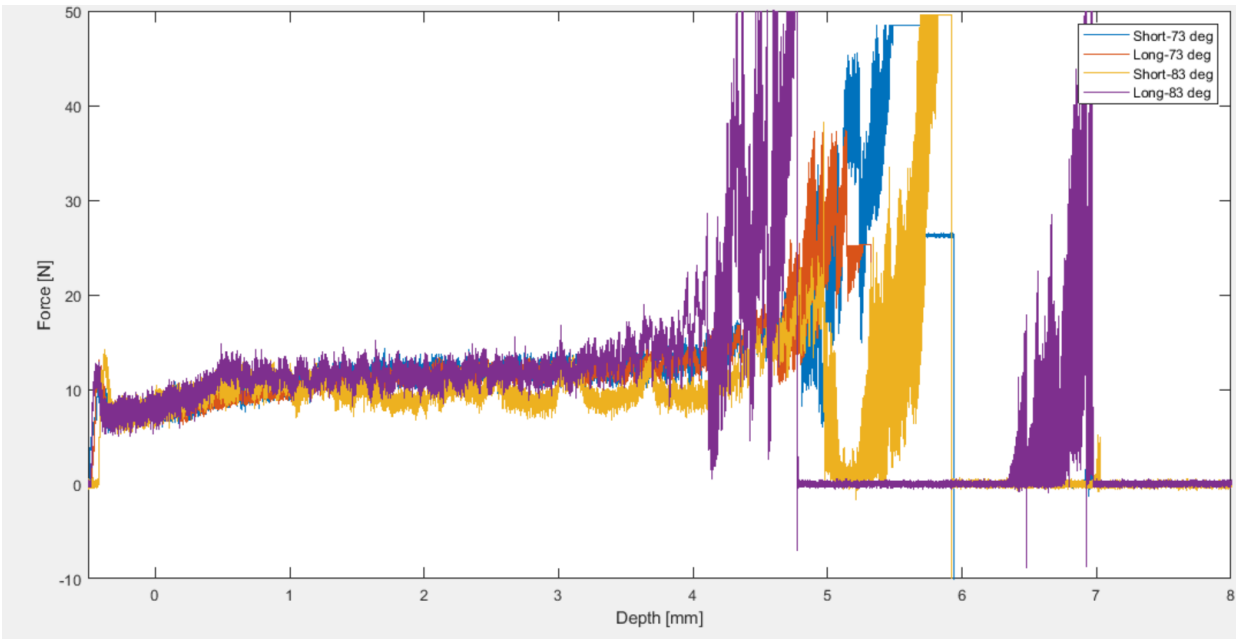
(d) Long Spray Distance



(e) Characteristic Curves for 73 degrees



(f) Characteristic Curves for 83 degrees

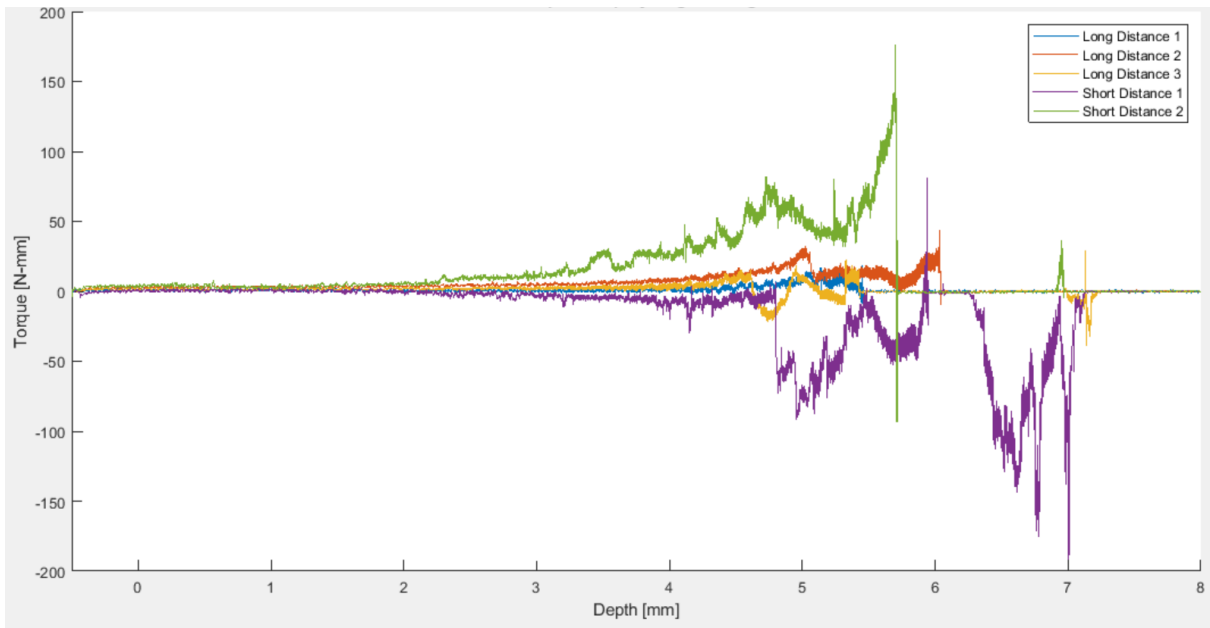


(g) All Characteristic Curves

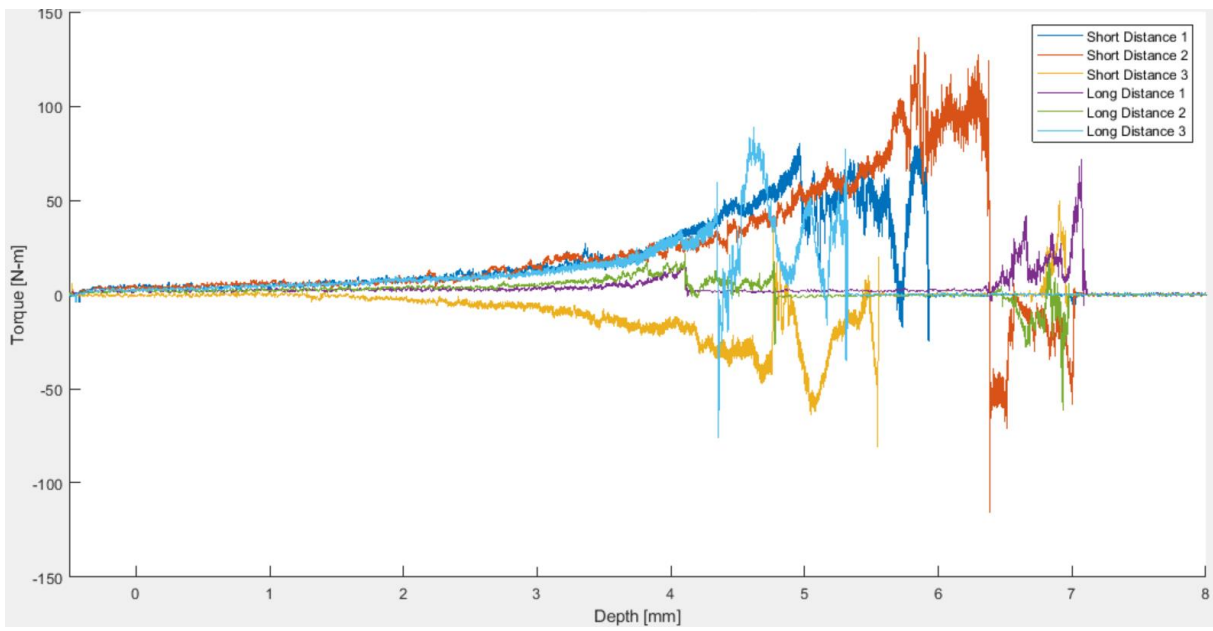
Figure 19: Cutting Force Progression with Respect to Drill Depth

5.3 Effect on Torque

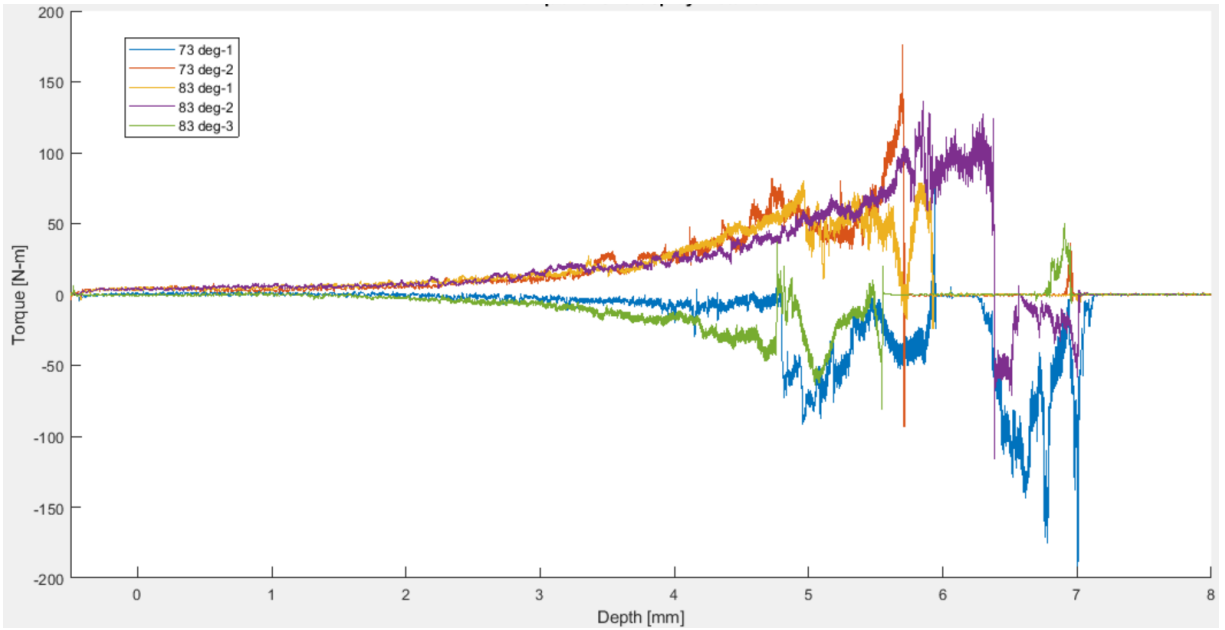
Torque plots for all experimental conditions are shown in Figure 20. Generally, the magnitude of torque increases more quickly for short spray distances. This may be because the spray is more concentrated near the atomizer output, and therefore drill bits closer to the atomizer output experience a stronger force due to the spray, and in turn, more significant torque. While most data show an exponential increase in torque throughout the drilling operation, some cases (e.g, short distance 3, 83 degrees case) exhibit unusual behavior, making the effects of spray angle and distance on torque unclear.



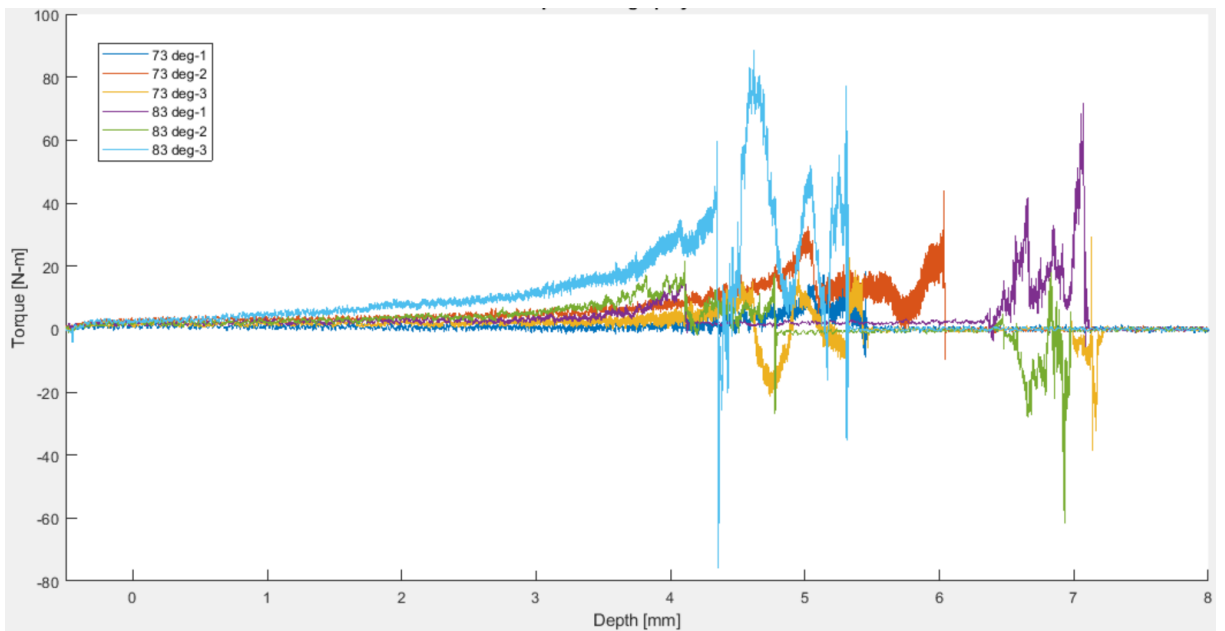
(a) Torque Progression for Spray Angle 73 degrees



(b) Torque Progression for Spray Angel 83 degrees



(c) Short Spray Distance



(d) Long Spray Distance

Figure 20: Torque with Respect to Drill Depth

5.4 Effects on Tool Life

Finally, the tool life for each experiment is estimated from the force data. The location at which a sudden significant drop in cutting force occur indicates a tool breakage as shown in Figure 21. The estimated tool life for each experiment is summarized in Table 9. The average tool life for 73-degree, 83-degree, short-distance, and long-distance cases are all longer than the average for the dry drilling case. Comparing the

average tool lives for the two different spray angles tested, the 73-degree case resulted in a 4.5% longer tool life compared to the 83-degree case. Comparing the short and long spray distances, the short spray distance case resulted in a tool life that is 10.7% longer than for the long spray distance case. These results suggest that the spray distance has a more significant effect on tool life than spray angle, and that shorter distance between the drill bit and the spray result in maximum tool life.

However, this relationship is questionable for multiple reasons. Firstly, the tool life varies greatly for different trials of the same test condition. For example, for the 83-degree, short distance case, tool lives 4.98, 5.87, and 4.78 mm are obtained. Secondly, while the two spray distances tested are significantly different, the two spray angles tested are rather similar. It may be possible that the effects of spray angle become more apparent for highly distinct angle values.

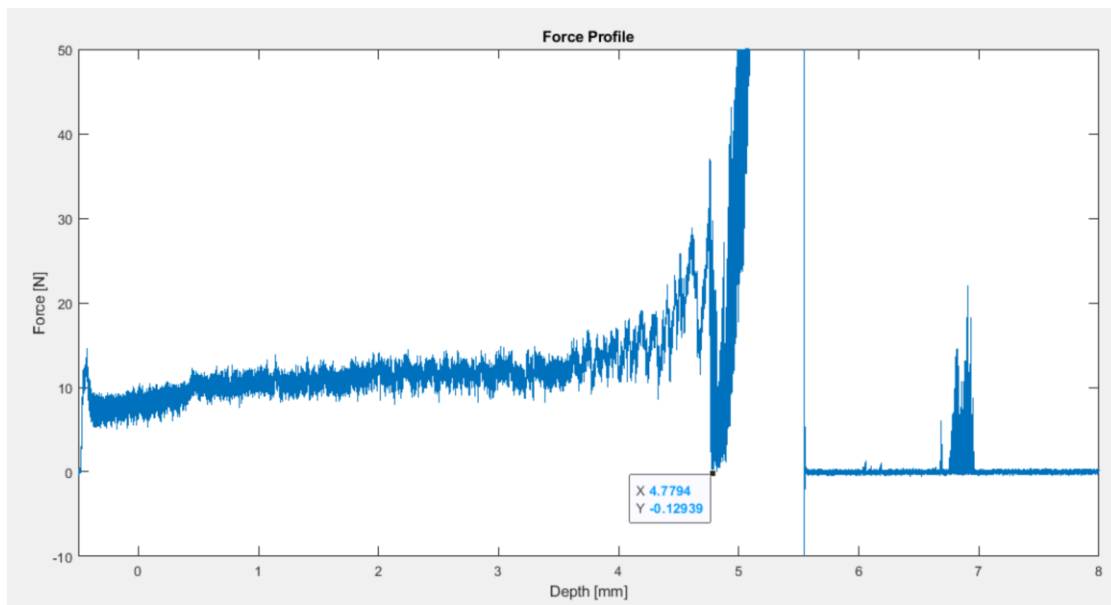


Figure 21: Example of Tool Life Definition (4.78 mm)

Table 9: Tool Life

Experiment #	Spray Angle [deg]	Spray Distance	Tool Life [mm]
Dry 1	73	-	4.23
Dry 2	73	-	4.46
1	73	Short	4.80
2	73	Short	4.97
3	73	Long	5.16
4	73	Long	5.07
5	73	Long	4.63
6	83	Short	4.98
7	83	Short	5.87
8	83	Short	4.78
9	83	Long	4.11
10	83	Long	4.14
11	83	Long	4.43
Dry Average	-	-	4.35
Short Distance Average	-	Short	5.08
Long Distance Average	-	Long	4.59
73 degrees Average	73	-	4.93
83 degrees Average	83	-	4.72

6. Conclusions

This project investigated the effects of ACF spray distance and angle on cutting force, torque, and tool life in a micro-drilling operation. The four test conditions using two different spray angles and distances resulted in similar force profiles, but distinct torque profiles and tool life. Results suggest the following relationships:

1. Shorter distance between the ACF spray and the drilling interface results in higher torque:
A likely cause for this effect is the high concentration of the spray near the outlet of the atomizer. A drill bit near the atomizer outlet experiences a larger force from the concentrated flow, while a bit further away from the outlet experiences less force because the spray is more dispersed.
2. Shorter distance also results in longer tool life:
This may be a result of more effective cooling and lubrication due to the high droplet impact rate (as a result of higher spray density).

3. A less-horizontal spray angle result in longer tool life:

While the observed effect is small, less-horizontal spray angle may result in better chip removal, contributing to increased tool life.

7. Recommendations

Following future work may expand the knowledge on the effects of ACF spray parameters on its performance during micro-drilling:

- Additional trials for experiments performed in this project to confirm the relationships discussed in conclusions, and to investigate whether an optimal distance and angle exists.
- Shorter spray distance resulted in long tool life, but also large torque, which is potentially a result of droplet impact. The effects of spray droplet size on torque may be studied to investigate whether smaller droplet size can reduce the torque while keeping a short spray distance.
- The effects of additional factors such as cutting fluid type, fluid flow rate, air pressure, feed rate, drill rotational speed, and compatibility between drill and workpiece materials, may be investigated.

References

- [1] Maruda, Radoslaw W., et al. "A Study on Droplets Sizes, Their Distribution and Heat Exchange for Minimum Quantity Cooling Lubrication (MQCL)." *International Journal of Machine Tools and Manufacture*, vol. 100, Jan. 2016, pp. 81–92., doi:10.1016/j.ijmachtools.2015.10.008.
- [2] Jun, Martin B. G., et al. "An Experimental Evaluation of an Atomization-Based Cutting Fluid Application System for Micromachining." *Journal of Manufacturing Science and Engineering*, vol. 130, no. 3, Dec. 2008, doi:10.1115/1.2738961.
- [3] Nath, Chandra, et al. "Design and Evaluation of an Atomization-Based Cutting Fluid Spray System in Turning of Titanium Alloy." *Journal of Manufacturing Processes*, vol. 14, no. 4, Sept. 2012, pp. 452–459., doi:10.1016/j.jmapro.2012.09.002.
- [4] Ganguli, Surojit, and Shiv G. Kapoor. "Improving the Performance of Milling of Titanium Alloys Using the Atomization-Based Cutting Fluid Application System." *Journal of Manufacturing Processes*, vol. 23, June 2016, pp. 29–36., doi:10.1016/j.jmapro.2016.05.011.
- [5] Rajan, R., and A.b. Pandit. "Correlations to Predict Droplet Size in Ultrasonic Atomisation." *Ultrasonics*, vol. 39, no. 4, 2001, pp. 235–255., doi:10.1016/s0041-624x(01)00054-3.
- [6] Liu, Z Q, et al. "Investigation of Cutting Force and Temperature of End-Milling Ti–6Al–4V with Different Minimum Quantity Lubrication (MQL) Parameters." *Proceedings of the Institution of Mechanical Engineers, Part B: Journal of Engineering Manufacture*, vol. 225, no. 8, 2011, pp. 1273–1279., doi:10.1177/2041297510393793.
- [7] Tanveer, Asif, et al. "A Thermal Model to Predict Tool Temperature in Machining of Ti-6Al-4V Alloy With an Atomization-Based Cutting Fluid Spray System." *Volume 1: Processing*, 2016, doi:10.1115/msec2016-8595.
- [8] Perçin, M., et al. "Micro-Drilling of Ti–6Al–4V Alloy: The Effects of Cooling/Lubricating." *Precision Engineering*, vol. 45, 7 Mar. 2016, pp. 450–462., doi:10.1016/j.precisioneng.2016.02.015.
- [9] Ghai, Isha, et al. "Droplet Behavior on a Rotating Surface for Atomization-Based Cutting Fluid Application in Micromachining." *Journal of Manufacturing Science and Engineering*, vol. 132, no. 1, Mar. 2010, doi:10.1115/1.4000859.
- [10] Ultrasonic atomizers. Newtown, CT, USA: Sonics and Materials, Inc. <http://www.sonics.com/liquid-datasheet/Atomizers.pdf>
- [11] STAVAX ESR, ASSAB, Singapore, Accessed on: November 9, 2019. [Online]. Available: http://www.assab-singapore.com/media/Stavax_ESR.pdf
- [12] Performance Micro Tool INNOVATION RULES Product Catalog. Performance Micro Tool., Janesville, WI, USA. Accessed on: November. 9, 2019. [Online]. Available: <http://www.pmtnow.com/pdf/2012-PMT-Catalog.pdf>

Appendix

Diameter, Web Thickness, and Land Calculation Function

```
def find_corner1(coords, center, crop_h):
    possible_corner = []
    center_x = center[0]
    center_y = center[1]
    h_low = crop_h[0]
    i = center_y
    corner = center
    while (i >= h_low):
        for coord in coords:
            if coord[1] == i:
                if center_x - coord[0] >= 20:
                    possible_corner.append(coord)
        if len(possible_corner) == 0:
            return corner
        else:
            sorted_corners = sorted(possible_corner,
key=itemgetter(0))
            corner = sorted_corners[0]
            possible_corner = []
            i -= 1

def find_corner2(coords, center, crop_h):
    possible_corner = []
    center_x = center[0]
    center_y = center[1]
    h_high = crop_h[1]
    i = center_y
    corner = center
    while(i <= h_high):
        for coord in coords:
            if coord[1] == i:
                if coord[0] - center_x >= 20:
                    possible_corner.append(coord)
        if len(possible_corner) == 0:
            return corner
        else:
            sorted_corners = sorted(possible_corner,
key=itemgetter(0))
            corner = sorted_corners[-1]
            possible_corner = []
            i += 1

def calc_diameter_web_land(filename, crop_h, crop_w):
    image = cv2.imread(filename)
    crop = image[crop_h[0]:crop_h[1], crop_w[0]:crop_w[1]]
    crop = cv2.cvtColor(crop, cv2.COLOR_BGR2GRAY) # convert to grayscale
    blur = cv2.GaussianBlur(crop, (13, 13), 0) # Blur

    lowerTh = 75
    upperTh = 255

    mask = cv2.inRange(blur, lowerTh, upperTh) # apply brightness
threshold
```

```

mask = cv2.erode(mask, None, iterations=2) # erode (eliminate noise)
mask = cv2.dilate(mask, None, iterations=3) # dilate (fill in missing
pixels)

#cv2.imshow('mask',mask)

whitepix = cv2.findNonZero(mask) # find all white pixel coordinates

# Extract white pixel coordinates
coords = []

for element in whitepix:
    coords.append([element[0][0],element[0][1]])

sort_y = sorted(coords, key=itemgetter(1)) # Sort by y (low2high)

# Get Top point (P1) and Bottom point (P2)
P_top = sort_y[0]
P_bottom = sort_y[-1]

# Get Center
center_x = int(0.5*(P_top[0]+P_bottom[0]))
center_y = int(0.5*(P_top[1]+P_bottom[1]))
center = [center_x,center_y]

# Get Corners for Web Thickness
corner1 = find_corner1(coords,center,crop_h)
corner2 = find_corner2(coords,center,crop_h)
web = np.sqrt((corner1[0]-corner2[0])**2 + (corner1[1]-corner2[1])**2)

#Calculate Diameter
vertical = np.absolute(P_top[1]-P_bottom[1])
horizontal = np.absolute(corner1[0]-corner2[0])
diameter = np.sqrt(vertical**2 + horizontal**2)

# Calculate Land
sort_x = sorted(coords, key=itemgetter(0)) # Sort by x (low2high)
land_point = sort_x[0]
land = np.sqrt((land_point[0]-P_bottom[0])**2 + (land_point[1]-
P_bottom[1])**2)

return diameter, web, land

```

Point Angle Calculation Function

```

def calc_point_ang(filename,crop_x): # Input image file and crop range
    image = cv2.imread(filename) # read file
    # Brightness Threshold
    lowerTh = 90
    upperTh = 255

    image = cv2.cvtColor(image,cv2.COLOR_BGR2GRAY) # convert to grayscale
    mask = cv2.inRange(image, lowerTh, upperTh) # convert to binary
    mask = cv2.erode(mask, None, iterations=3) # erode (eliminate noise)
    mask = cv2.dilate(mask, None, iterations=2) #
    inv = cv2.bitwise_not(mask) # invert

```

```

crop = inv[0:h,crop_x[0]:crop_x[1]] # crop to get tip only
whitepix = cv2.findNonZero(crop) # get coordinates of white pixels

# Extract coordinates of white pixels
coords = []
x = []
y = []

for element in whitepix:
    coords.append([element[0][0],element[0][1]])
    x.append(element[0][0])
    y.append(element[0][1])

# Find Triangle Vertices
minx_index = x.index(min(x))
miny_index = y.index(min(y))
minx_point = coords[minx_index]
miny_point = coords[miny_index]

# Solve for point angle
point_ang = 2*np.arctan(np.absolute(minx_point[1]-
miny_point[1])/np.absolute(minx_point[0]-miny_point[0]))
point_ang = np.degrees(point_ang)

return point_ang

```

Helix Angle Calculation Function

```

def calc_helix_ang(filename,crop_x,crop_y):
    image = cv2.imread(filename) # read file
    image = cv2.cvtColor(image,cv2.COLOR_BGR2GRAY) # convert to grayscale
    crop = image[crop_y[0]:crop_y[1],crop_x[0]:crop_x[1]] # crop image
    blur = cv2.GaussianBlur(crop, (5,5),cv2.BORDER_DEFAULT) # blur
    # Define Brightness Threshold
    lowerTh = 100
    upperTh = 255

    mask = cv2.inRange(crop, lowerTh, upperTh) # convert to binary
    mask = cv2.erode(mask, None, iterations=2) # erode
    mask = cv2.dilate(mask, None, iterations=3) # dialate
    whitepix = cv2.findNonZero(mask) # get white pixel coordinates

    # Extract coordinates of white pixels
    coords = []

    for element in whitepix:
        coords.append([element[0][0],element[0][1]])

    sorted_coords = sorted(coords, key=itemgetter(0)) # x low2high
    point1 = sorted_coords[0:50] # Take first 50
    point1 = sorted(point1, key=itemgetter(1),reverse=True) # y high2low
    [x1,y1] = [point1[0][0],point1[0][1]] # Point 1

    sorted_coords2 = sorted(coords, key=itemgetter(1),reverse=True)
    point2 = sorted_coords2[0:50] # Take first 50

```

```

point2 = sorted(point2, key=itemgetter(0)) # x low2high
[x2,y2] = [point2[0][0],point2[0][1]] # Point 2

# Calculate Helix Angle
helix_ang = np.arctan((y2-y1)/(x2-x1))
helix_ang = np.degrees(helix_ang) # Convert to degrees

return helix_ang

```

Data Preprocessing

```

function no_drift = remove_drift(data,dref)

% This function removes drift by taking raw data and the indices of
% the data where a polynomial is fit

dr = [data(dref(1,1):dref(1,2));data(dref(2,1):dref(2,2))]; % sections of raw
data where a curve will be fit
xd = 0:1:length(data)-1;
drx = [(dref(1,1):1:dref(1,2))';(dref(2,1):1:dref(2,2))'];
coeff = polyfit(drx,dr,2); % coefficients of a 2nd degree polynomial of best
fit
curve = polyval(coeff,xd); % the generated curve
no_drift = data - curve'; % drift correction

end

```